Vrehen, Q. H. F.
Volger, J.
1965

Physica 31
845–865

PARAMAGNETIC RESONANCE OF DIVALENT EUROPIUM IN LEAD CHLORIDE *)

by Q. H. F. VREHEN **) and J. VOLGER

Fysisch Laboratorium der Rijksuniversiteit, Utrecht, Nederland

Synopsis

Paramagnetic resonance spectra of Eu^{2+} ions at Pb^{2+} sites in $PbCl_2$ were measured at room temperature and 3 cm wavelength. The point group symmetry at a Pb^{2+} site is monoclinic. Apart from a reflection, all sites in the unit cell are magnetically equivalent. Analysis yielded the following values for the dominant parameters in the spin Hamiltonian:

$$g = 1.993 \pm 0.003 \text{ isotropic}$$
$$b_2^0 = (+107 \pm 1) \times 10^{-4}\,\text{cm}^{-1}$$
$$b_2^2 = (-527 \pm 2) \times 10^{-4}\,\text{cm}^{-1}$$

The z-axis is along the crystallographic a axis, x and y axes 23.5° from the crystallographic b and c axis respectively. In order to obtain a fit with the measured hyperfine structure for ^{151}Eu terms $\Sigma_i A_i' S_i^3 I_i$ are added to the spin Hamiltonian. The values for the HFS parameters are (in units $10^{-4}\,\text{cm}^{-1}$):

$$^{151}A_x = -31 \pm 1 \qquad ^{151}A_x' = -0.10 \pm 0.02$$
$$^{151}A_y = -33.0 \pm 0.5 \qquad ^{151}A_y' = +0.10 \pm 0.02$$
$$^{151}A_z = -33.6 \pm 0.5 \qquad ^{151}A_z' = +0.11 \pm 0.02$$
$$^{153}Q_1 = +0.33 \pm 0.06$$
$$|^{153}Q_2| = +3.8 \pm 0.1$$

The results are interpreted in terms of crystal field theory. Evidence is presented indicating that the second degree crystal field splittings found are mainly linear in the field strength. Under the assumption that a perturbation mechanism, linear in field strength and cubic in spin-orbit coupling, is mainly responsible for the second degree crystal field splittings, a value is derived for the electronic shielding coefficients γ_∞ and γ_2. The result is $(1 - \gamma_\infty)/(1 - \gamma_2) = +169$, in reasonable agreement with present theoretical estimates.

1. *Introduction.* Second degree crystal field splittings, i.c., those corresponding to parameters b_2^0 and b_2^2 in the spin Hamiltonian, of the electronic configuration $4f^7\ ^8S_{7/2}$ have been investigated in the past for Gd^{3+} in axial

*) This paper presents in an abbreviated form, part of the first author's thesis[1]).

**) Now at National Magnet Laboratory, Massachusetts Institute of Technology, Cambridge 39. Massachusetts, U.S.A.

crystals[2]). Perturbation mechanisms accounting for these splittings have been proposed by Pryce[3]), Elliott and Stevens[4]) and Judd[5]). For the first two of these mechanisms the splittings depend linearly on the second degree crystal field strengths, whereas for the third one the splittings are quadratic functions of the crystal fields and other than second degree fields may contribute. Lack of knowledge of the crystal field strengths complicates the comparison of experimental with theoretical results. A further complication arises from the fact that electronic shielding causes the effective field experienced by the $4f$ electrons to differ from the external crystalline electric field. The electric field gradient at the nucleus is also greatly affected by polarization effects (Sternheimer shielding or anti-shielding factor).

In the present paper we describe *PMR* measurements on Eu^{2+} in $PbCl_2$ and an interpretation of the results in terms of crystal field theory. These measurements stand out from those for Gd^{3+} in axial fields in two respects. First, the point group symmetry of a Pb^{2+} site in $PbCl_2$ is monoclinic. Therefore, two second degree splitting parameters are present in the spin Hamiltonian, an axial (b_2^0) and an orthorhombic (b_2^2) parameter. The ratio of two crystal field strengths of the same degree can often be calculated more reliably than the magnitude of each of them[6]). The presence of two parameters then permits one to check whether the splittings are linear in the crystal field strengths or not. (See appendix B.) Secondly, the two stable isotopes ^{151}Eu and ^{153}Eu have relatively large nuclear quadrupole moments. We were able to analyze the nuclear quadrupole interaction for ^{153}Eu, from which further information concerning the second degree crystal fields can be derived. It may be emphasized here that since Eu^{2+} is in an S-state there is no direct interaction between the nuclear quadrupole and the $4f$-shell. The electric field gradient at the nucleus is determined by the crystalline electric field and the antishielding factor γ_∞ (which in this case includes shielding due to the open $4f$ shell). A comparison of the experimental values of the fine structure splittings with those for the nuclear quadrupole interaction and with the computed values for the crystal field gradient tensor leads to the conclusion that b_2^0 and b_2^2 are mainly linear in the corresponding crystal field strengths. Under the assumption that the perturbation mechanism proposed by Elliott and Stevens[4]) is responsible for these linear splittings a value can be derived for the ratio $(1-\gamma_\infty)/(1-\gamma_2)$. This value is then compared with other recently determined theoretical and experimental values for this ratio.

The hyperfine interaction is usually represented in the spin Hamiltonian by three terms, the nuclear Zeeman energy, the quadrupole energy and the scalar interaction $A\boldsymbol{S}\cdot\boldsymbol{I}$ between nuclear and electron spins. In the present case it is found that the hyperfine splittings for ^{151}Eu cannot be fitted satisfactorily to such a Hamiltonian. Reasonable agreement can be

obtained by introducing terms $\sum_i A_i S_i^3 I_i$. Although the physical meaning of such terms is not well understood, we add them to the Hamiltonian in order to clearly indicate the character of the deviations.

The analysis of the experimental data makes use of the transformation properties of the spin Hamiltonian, which are discussed in appendix A. In appendix B a theorem is considered relating second degree crystal field parameters in the spin Hamiltonian to second degree crystal field strengths.

2. *Experiment.* All *PMR* measurements were made at room temperature and at 3 cm wavelength. A hybrid tee bridge circuit and straight detection were used, the magnetic field modulation being at either 63 Hz or 935 Hz. The narrowest lines observed had a width of approximately 5 gauss (at half height) and the modulation depth was kept sufficiently small to avoid distortion of line shapes. Cylindrical cavities TE 011 and rectangular cavities TE 102 were used. The spectrometer had a sensitivity of approximately 4×10^{12} spins/gauss for a klystron power of 10 mW and a response time of 10 s at the higher modulation frequency.

The magnet was built in the workshop of our laboratory; it has a gap of 6 cm with a pole diameter of 15 cm; the maximum field strength is about 7000 gauss for a 15*A* current through the 6 ohm magnet windings. The magnet current was stabilized with a circuit similar to one by Garwin[7][8]; a magnetic field stability of about $1 : 10^5$ both long and short term was obtained in this way. The current could be varied linearly from zero to its maximum value with corresponding field variations of approximately 20 gauss/minute and 200 gauss/minute.

Between 1600 gauss and 4500 gauss the magnetic field could be measured with a proton resonance magnetometer; outside this range fields were determined by extrapolation. With the help of the resonance of a small amount of *DPPH* attached to the sample under investigation corrections could be made for the field difference between the proton sample and the crystal on which the *PMR* measurements were made.

Single crystals $PbCl_2$ containing a small amount of Eu were prepared by Mr. K. J. de Vries of our laboratory, by a slightly modified Stockbarger technique. A semiquantitative spectrochemical analysis of such a Eu doped crystal was made at Philips' Natuurkundig Laboratorium at Eindhoven. A Ca concentration of 0.03% (weight) was found; all other metals except Eu had a concentration smaller than 0.01%. The Eu concentration was not determined. From the intensity of the *PMR* signals we estimated this concentration to be about 0.1%, whereas roughly 1% had been added to the melt.

$PbCl_2$ has a cleavage plane perpendicular to its *c* axis[9]. (This was confirmed by a measurement of the lattice constant for the direction normal

to the cleavage plane. The result was 9.00 ± 0.05 Å.) Samples were prepared as plates 0.2 to 0.3 cm thick perpendicular to the c axis. The directions of a and b axis could now easily be found with the help of a polarization microscope. Faces were ground on the samples perpendicular to these axes. Subsequently the sample was glued to a quartz bar with one of its axes parallel to the bar. By rotating the bar *PMR* spectra could be recorded with the magnetic field in the *ab*, *ac*, or *bc* plane.

3. *Crystal structure of $PbCl_2$ and calculation of the electric field gradient at a Pb^{2+} site.* The crystal structure of $PbCl_2$ has been studied by Braekken[10]). Recently, these measurements have been repeated by Sahl and Zemann[11]). These authors confirm Braekken's results, but they determined the position of the ions within the unit cell with greater accuracy. We follow Braekken's notation; in the calculations we used the values by Sahl and Zemann for the positions of the ions within the unit cell.

The space lattice of $PbCl_2$ is orthorhombic, $a = 4.525$ Å, $b = 7.608$ Å and $c = 9.030$ Å. The space group is D_{2h}^{16}. There are four molecules in the unit cell. Their positions can be given as:

$$\text{I}\begin{cases} P = (\tfrac{3}{4}, \tfrac{3}{4} + u, v) \\ Q = (\tfrac{1}{4}, \tfrac{1}{4} - u, -v) \end{cases} \qquad \text{II}\begin{cases} R = (\tfrac{3}{4}, \tfrac{1}{4} + u, \tfrac{1}{2} - v) \\ S = (\tfrac{1}{4}, \tfrac{3}{4} - u, -\tfrac{1}{2} + v) \end{cases}$$

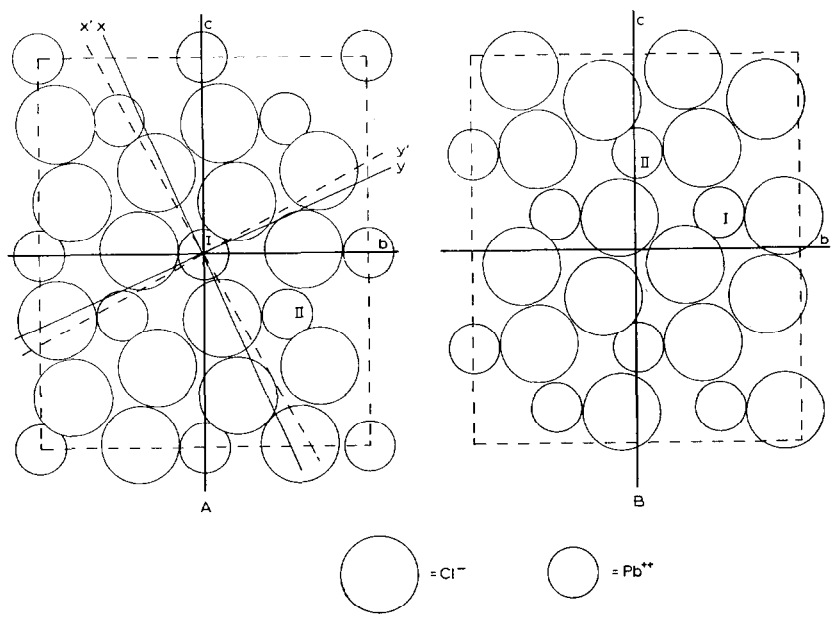

Fig. 1. Positions of the ions in the $PbCl_2$ lattice, (*a*) in a plane (100) and (*b*) in a plane (200). A lead ion of type Q is at the origin. x and y are axes found from the *PMR* spectrum, x' and y' are found from the crystal field calculation.

where for Pb^{2+} $u_0 = -0.014$, $v_0 = 0.096$ and for Cl^- $u_1 = 0.389$, $v_1 = 0.075$ and $u_2 = 0.273$, $v_2 = 0.663$. In fig. 1 a lead ion of type Q is taken at the origin. The position of the surrounding ions is sketched in the planes (100) and (200).

The point group at a Pb^{2+} site contains only two symmetry elements: the identity and the reflection through the bc plane. The point group is monoclinic C_s. The experimental results are consistent with the assumption that the Eu^{2+} ion is built-in in the $PbCl_2$ lattice substitutionally for Pb^{2+}. By the inversion, followed by an appropriate translation P can be made to coincide with Q. For this reason sites P and Q are magnetically equivalent. Their PMR spectra are identical; we shall call them sites I. For the same reason sites R and S are magnetically equivalent; we call them sites II.

Sites I can be transformed into sites II by a reflection through the ab or ac plane followed by an operation that leaves the site magnetically unchanged. From these considerations the following may be concluded:

a. For the magnetic field in the ab or ac plane the PMR spectra of sites I and II coincide.

b. If the magnetic field is in the bc plane the PMR spectra of sites II can be found from those of sites I by a reflection through the b or c axis.

The second degree part of the crystalline electric field at a Pb^{++} site may be written as:

$$V_2 = C_2^0(3z'^2 - r^2) + C_2^2(x'^2 - y'^2) \tag{1}$$

where x', y', and z' are the principal axes. From the symmetry it follows that one of these axes (say z') is along the crystallographic a axis; x' and y' are in the bc plane. In the point charge approximation we have:

$$C_2^0 = \frac{1}{16\pi\varepsilon_0} \sum_j{}' \frac{q_j}{r_j^5}(3z_j'^2 - r_j^2) \tag{2}$$

The summation is over all ions in the lattice except the one at the site of which the field is calculated. A similar expression holds for C_2^2. These expressions are too slowly convergent for practical use. We calculated C_2^0 and C_2^2 for a lattice site of type Q with the help of rapidly converging expressions derived by Nijboer and de Wette[12]). We found *)

$$C_2^0 = (+2.7 \pm 2) \times 10^{18}\ \mathrm{V/m^2} \qquad A_2^0 = -61 \pm 45\ \mathrm{cm^{-1}}/a_0^2$$
$$C_2^2 = (-17 \pm 3) \times 10^{18}\ \mathrm{V/m^2} \qquad A_2^2 = +384 \pm 68\ \mathrm{cm^{-1}}/a_0^2$$

x' and y' lie 30°.5 from c and b axis respectively (see fig. 1). The A_l^m are defined as $A_l^m = -e\,C_l^m$, where e is the proton charge. a_0 is the atomic unit of length. The uncertainties in the parameters as indicated above

*) In the actual calculation we used V_2 in the nondiagonal form, taking coordinate axes along the crystallographic axes. The result was then transformed to the principal axes.

are due to uncertainties in the X ray data. Insufficiency of the point charge model might, of course, introduce much larger errors.

The case of Eu^{2+} in $PbCl_2$ seems favorable for the calculation of the crystalline electric field for the following reasons.

a. The X ray data for $PbCl_2$ are accurately known.

b. $PbCl_2$ has to a reasonable extent ionic character[13]).

c. $EuCl_2$ is isomorphous with $PbCl_2$ and has nearly the same lattice constants ($a = 4.525$ Å, $b = 7.608$ Å and $c = 9.030$ Å for $PbCl_2$[10]) and $a = 4.493$ Å, $b = 7.499$ Å and $c = 8.914$ Å for $EuCl_2$[14])).

d. Eu^{2+} has nearly the same radius as Pb^{2+} (1.17 Å for Pb^{++} and 1.14 Å for Eu^{2+})[15]).

From *a* and *b* we infer that the field at a Pb^{2+} site might be fairly well calculated, whereas from *c* and *d* it may be concluded that the introduction of 0.1% $EuCl_2$ into $PbCl_2$ will give only a small distortion of the $PbCl_2$ lattice and thus the field at a Eu^{2+} site will almost equal the field at a Pb^{2+} site in pure $PbCl_2$.

4. *The spin Hamiltonian.* We interpreted our experimental results in terms of the following spin Hamiltonian:

$$\mathcal{H} = \beta(g_x H_x S_x + g_y H_y S_y + g_z H_z S_z) + \sum_{\substack{l=2 \\ \text{even}}}^{6} \sum_{\substack{m=0 \\ \text{even}}}^{l} (B_l^m O_l^m + B_l^{-m} O_l^{-m}) +$$
$$+ \sum_{i=x,y,z} A_i S_i I_i + \sum_{i=x,y,z} A_i' S_i^3 I_i +$$
$$+ Q_1(3I_z^2 - I(I+1)) + \tfrac{1}{2} Q_2(I_+^2 + I_-^2) + g_I \beta \boldsymbol{H} \cdot \boldsymbol{I}. \qquad (3)$$

Terms in the first line represent the electronic Zeeman energy and crystal field energy. The second line describes the interaction between the electronic and nuclear magnetic moment whereas the third line gives the terms for the interaction of the nuclear quadrupole moment and the electric field gradient at the nucleus and the Zeeman energy of the nuclear magnetic moment.

The O_l^m are the well known operator equivalents[16]). Expressions for these operators as well as for their matrix elements within certain manifolds of angular momentum may be found in the literature[16–21]). The O_l^{-m} can be obtained from the O_l^m by substituting $-i(S_+^k - S_-^k)$ for $(S_+^k + S_-^k)$. For the matrix elements we have therefore:

$$\langle M'|O_l^{-m}|M\rangle = -i\langle M'|O_l^m|M\rangle \text{ for } M' > M,$$
$$\langle M'|O_l^{-m}|M\rangle = \quad i\langle M'|O_l^m|M\rangle \text{ for } M' < M.$$

Introduction of the O_l^{-m} is necessary in the present case because of the low point group symmetry at the magnetic ion site.

In the expression for the spin Hamiltonian the z axis has been chosen

along the crystallographic a axis. We define x and y axis by the requirements $B_2^{-2} = 0$ and $B_2^2/B_2^0 < 0$.

Strictly speaking g and A are symmetrical tensors having one of their principal axes along the z axis, the other two in the xy plane but not necessarily coinciding with the x and y axis as assumed in eq. (3). As a result of bad resolution in many directions in the xy plane, the exact position of the principal axes in this plane could not be determined. It was found, however, that g is isotropic within the accuracy of the measurements and that A is only slightly anisotropic. On account of this small anisotropy we are justified in performing the calculations as if the principal axes of g and A were along x, y, z. The same type of difficulty arises with respect to the quadrupole interaction. The expression used in eq. (3) suggests that the principal axes of the crystal field gradient were along x, y, and z. Experimentally the quadrupole interaction could be studied only for H along the z axis. Therefore, the principal axes of the electric field gradient in the xy plane could not be determined experimentally and the expression used in eq. (3) is the simplest one for the interpretation of the results for H along z.

We now proceed to describe how the parameters in the Hamiltonian were determined from the experimental results. For an allowed transition the selection rule $\Delta M = \pm 1$, $\Delta m = 0$ holds, M and m being the electronic and nuclear magnetic quantum numbers respectively. Let $H(M, m, \theta, \varphi)$ be the magnetic field at which the resonance $M \leftrightarrow M-1$, $I_z = m$ takes place, H being in the direction (θ, φ), and $H(M, \theta, \varphi)$ the field at which the resonance would occur if hyperfine interaction were absent.

Since the crystal field splittings are smaller than the Zeeman splittings, the energy levels could be calculated by perturbation theory. First and second order perturbation formulae are given in appendix A. It turned out that, for the choice of x and y axis so that $B_2^{-2} = 0$ all parameters B_l^{-m} are relatively small. From expressions (8) and (9) it can be seen that for H along x, y, and z axis the terms in the B_l^{-m} may then be neglected. For these directions therefore the $H(M, \theta, \varphi)$ were equated to expressions in g_x, g_y, g_z and the B_l^m. Some third and fourth order terms were included. Using estimates for the second and higher order terms we are left with 21 linear equations (7 resonance lines in each of 3 directions) for the 12 parameters. These equations were solved by the method of least squares using the University's ZEBRA computer. Better estimates of the higher order terms could then be made and the process repeated until a consistent solution was obtained. In these calculations B_2^0 was assumed to be positive.

The B_l^{-m} were computed by studying the experimentally determined functions

$$H_{\text{odd}}\left(M, \frac{\pi}{2}, \varphi\right) = \frac{1}{2}\left(H\left(M, \frac{\pi}{2}, \varphi\right) - H\left(M, \frac{\pi}{2}, -\varphi\right)\right)$$

By equating these functions to the first and second order perturbations in B_l^{-m} (see eqs. (8) and (9)) and by again performing a least square analysis, the values of the B_l^{-m} were found.

There are two stable isotopes, ^{151}Eu and ^{153}Eu of nearly equal abundance (47.86 and 52.14 percent) and both with nuclear spin $I = \frac{5}{2}$. The nuclear magnetic moments are[22]) 3.44*nm* and 1.52*nm*, the quadrupole moments[23]) 0.95×10^{-24} cm^2 and 2.42×10^{-24} cm^2 respectively.

To first order the terms in A_x, A_y, A_z split each electronic resonance line into two groups of six equally spaced lines. For ^{151}Eu the spacings are about 2.25 times as large as for ^{153}Eu and both groups are centered at the same magnetic field. As a result the resolution of the *HF* pattern was bad for most electronic transitions. Often only the overall *HF* splitting, i.e., the separation between the outermost *HF* lines corresponding to $m = \frac{5}{2}$ and $m = -\frac{5}{2}$ for ^{151}Eu could be measured accurately. However, the resolution in the *HF* pattern of the transition $M = \frac{1}{2} \leftrightarrow M = -\frac{1}{2}$ for $H||z$ axis was good and thus a more detailed analysis of this transition could be made. The experimental data allowed us to determine A_x, A_y, A_z and A_x', A_y', A_z' for ^{151}Eu and Q_1, $|Q_2|$ for ^{153}Eu.

The overall splittings were fitted to the nuclear part of the Hamiltonian (3), taking into account second and third order effects[24–26]). Without the terms in A_i' no reasonable fit could be obtained, as will be shown in section 5. The analysis yielded values for the A_i and A_i' and a crude value of $|Q_2|$, all for ^{151}Eu.

The analysis of the *HF* pattern of the transition $M = \frac{1}{2} \leftrightarrow M = -\frac{1}{2}$ for $H||z$ yielded Q_1 and $|Q_2|$ for ^{153}Eu. For ^{151}Eu the term in A_z was found to be large compared to all other nuclear interactions, so that for this isotope the position of the allowed *HF* lines, together with the position and intensity of the forbidden lines (due to Q_2) could be calculated by the usual perturbation theory[24]). For ^{153}Eu on the other hand the term in A_z proved to be of the same order of magnitude as that in Q_2, whereas all other nuclear interactions were comparatively small. The usual perturbation theory in which $A_z S_z I_z$ is taken as the unperturbed Hamiltonian could not be applied. The intensity of the "allowed" lines was considerably smaller than that of some of the "forbidden" transitions. This state of affairs made the transition $M = \frac{1}{2} \leftrightarrow M = -\frac{1}{2}$ ideal for an accurate determination of Q_1 and $|Q_2|$ for ^{153}Eu. For our analysis we took the Hamiltonian

$$A_z S_z I_z + \tfrac{1}{2} Q_2 (I_+^2 + I_-^2) \tag{4}$$

as the unperturbed Hamiltonian and considered the remaining terms as perturbations. We assumed the ratio $^{151}A_z/^{153}A_z$ to be equal to 2.253 as found by Baker[22]) for Eu^{2+} in CaF_2. Since $^{151}A_z$ was already known from the overall splittings, this yielded $^{153}A_z$. We then diagonalized the Hamil-

tonian (4) numerically within the manifold $I = \frac{5}{2}$ for various values of Q_2. For each value of Q_2 the energies and wavefunctions of the HF levels for $M = \frac{1}{2}$ and for $M = -\frac{1}{2}$ were found and from these the intensity and position of the HF lines could be calculated. From a detailed comparison of the calculated spectra with the experimental one the value of $|Q_2|$ could be derived. The introduction of the terms in Q_1 and g_I gives rise to some further splittings of the HF lines. Since g_I was known from the literature[22]), Q_1 could be determined from these splittings. For this purpose the terms in Q_1 and g_I were added as perturbations to the Hamiltonian (4) and first order perturbation energies calculated.

5. *Experimental results. PMR* spectra were obtained for the magnetic field in the *ab*, *ac*, and *bc* planes. Figure 2 shows a typical spectrum for $H||a$. In order to make all electronic transitions clearly visible in this figure the low and high field lines have been recorded with larger gain than the central lines.

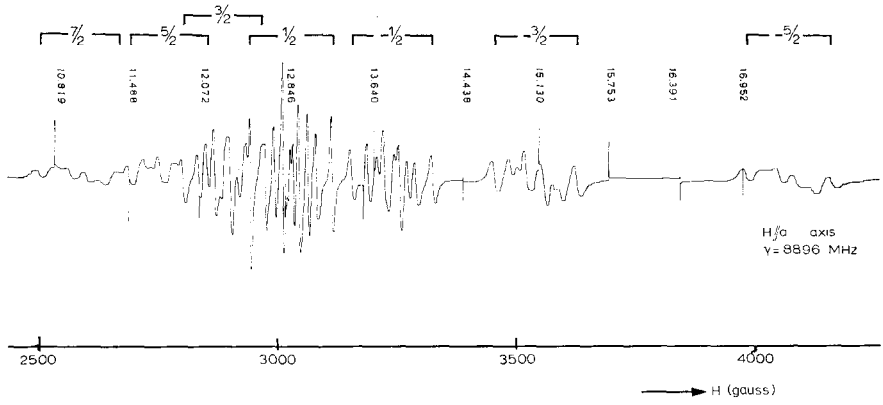

Fig. 2. Paramagnetic resonance spectrum of Eu^{2+} in $PbCl_2$ for the magnetic field parallel to the *a* axis. A line labelled M corresponds to the transition $M \leftrightarrow M-1$ (assumed $B_2^0 > 0$).

For each hyperfine group the magnetic field where the electronic transition would take place if the nuclear interaction were absent, was calculated. Rotational diagrams for the magnetic field in the *ab*, *ac*, and *bc* plane are given in figs. 3–6. As anticipated (Sec. 3) only one spectrum is observed for H in *ab* and *ac* plane whereas two spectra are present for H in the *bc* plane, one being the mirror image of the other with respect to the *b* (or *c*) axis. From the experiments it cannot be decided which spectrum belongs to site I and which to site II. The result of the crystal field calculation, however, suggests that the spectrum labelled I in fig. 5 should be assigned to site I (see sec. 3 and fig. 1). From figs. 3–6 the monoclinic

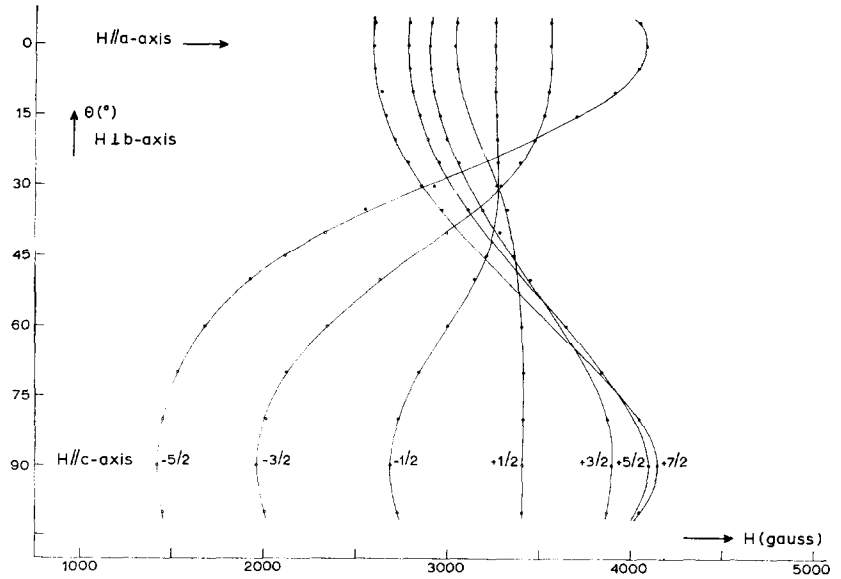

Fig. 3. Fine structure rotational diagram of the *PMR* spectrum of Eu^{2+} in $PbCl_2$. Rotation around *b* axis; *H* in the *ac* plane. A curve labelled *M* corresponds to transition $M \leftrightarrow M-1$ (assumed $B_2^0 > 0$).

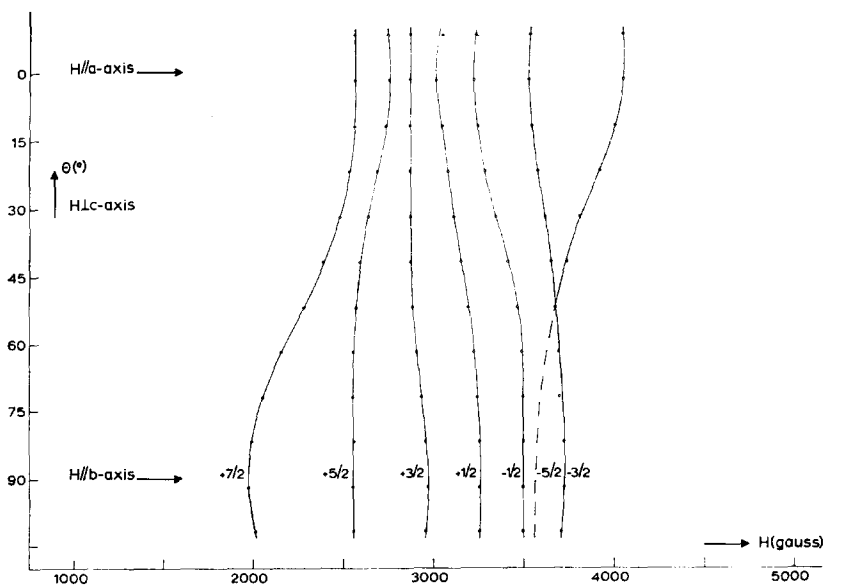

Fig. 4. Fine structure rotational diagram of the *PMR* spectrum of Eu^{2+} in $PbCl_2$. Rotation around *c* axis; *H* in the *ab* plane. A curve labelled *M* corresponds to the transition $M \leftrightarrow M-1$ (assumed $B_2^0 > 0$).

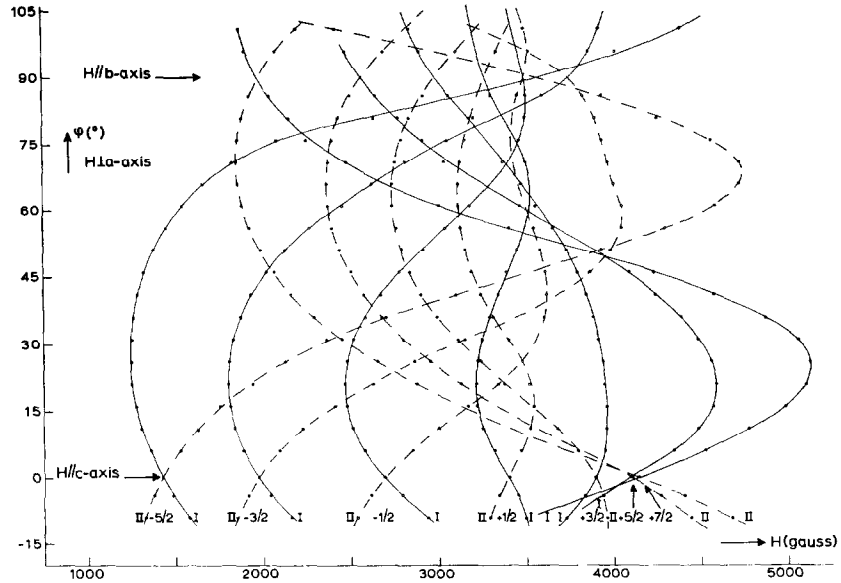

Fig. 5. Fine structure rotational diagram of the *PMR* spectrum of Eu^{2+} in $PbCl_2$. Rotation around *a* axis; *H* in the *bc* plane. I and II refer to the spectra for site I and II respectively. A curve labelled *M* corresponds to the transition $M \leftrightarrow M-1$ (assumed $B_2^0 > 0$).

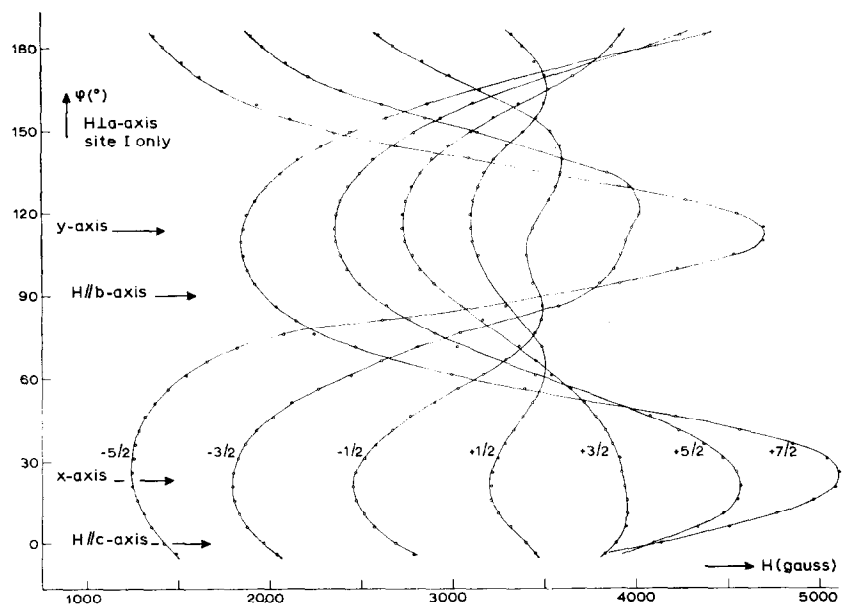

Fig. 6. Fine structure rotational diagram of the *PMR* spectrum of Eu^{2+} in $PbCl_2$. Rotation around *a* axis; *H* in the *bc* plane. Spectrum of site I only. *x* and *y* axis are found from the *PMR* spectrum (as defined in section 4).

TABLE I

g values and fine structure parameters for Eu^{2+} in $PbCl_2$ $b_2^{\pm m} = 3B_2^{\pm m}$; $b_4^{\pm m} = 60B_4^{\pm m}$; $b_6^{\pm m} = 1260B_6^{\pm m}$ The $b_l^{\pm m}$ are given in 10^{-4} cm^{-1}	
$g_x = 1.995 \pm 0.003$	
$g_y = 1.993 \pm 0.003$	
$g_z = 1.992 \pm 0.002$	
$b_2^0 = +107 \pm 1$	
$b_2^2 = -527 \pm 2$	$b_2^{-2} = 0 \pm 2$
$b_4^0 = +3.6 \pm 0.3$	
$b_4^2 = +1 \pm 2$	$b_4^{-2} = -6 \pm 2$
$b_4^4 = +26 \pm 2$	$b_4^{-4} = -26 \pm 3$
$b_6^0 = +0.4 \pm 0.4$	
$b_6^2 + b_6^6 = -5 \pm 5$	$b_6^{-2} = -2 \pm 4$
$b_6^4 = +2 \pm 6$	$b_6^{-4} = -14 \pm 10$
	$b_6^{-6} = -4 \pm 10$

TABLE II

HFS parameters for Eu^{2+} in $PbCl_2$ in 10^{-4} cm^{-1}	
$^{151}A_x = -31 \pm 1$	$^{151}A_x' = -0.10 \pm 0.02$
$^{151}A_y = -33.0 \pm 0.5$	$^{151}A_y' = +0.10 \pm 0.02$
$^{151}A_z = -33.6 \pm 0.5$	$^{151}A_z' = +0.11 \pm 0.02$
$^{153}Q_1 = +0.33 \pm 0.06$	
$\lvert^{153}Q_2\rvert = 3.8 \pm 0.1$	

TABLE III

Overall hyperfine splittings in the PMR spectrum of Eu^{2+} in $PbCl_2$ for $H \| a$ axis (in gauss)

Transition $M \leftrightarrow M-1$	Best fit for $^{151}A_z' = 0$	Best fit for $^{151}A_z' = (+0.11 \pm 0.02) \times 10^{-4}$ cm^{-1}	Experiment
7/2	173.5	166.7	168 ± 2
5/2	166.2	168.4	168 ± 2
3/2	161.5	168.1	169 ± 1
1/2	165.2	174.6	175 ± 1
−1/2	162.3	169.9	171 ± 1
−3/2	171.1	173.3	173 ± 1
−5/2	181.7	174.9	174 ± 2

symmetry at the Eu^{2+} sites becomes apparent. These data confirm the assumption that the Eu^{2+} enter the $PbCl_2$ lattice substitutionally for Pb^{2+}. Using the method of analysis described in sec. 4 the fine structure parameters as given in table I were obtained. The x and y axis were found to lie 23.5° from the c and b axis respectively. The positions of the electronic

transitions as calculated from these parameters were generally in good agreement with the experimental ones.

The analysis of *HFS* yielded the following values for the parameters (Table II). Without the terms $\sum A_i' S_i^3 I_i$ in the Hamiltonian the experimental overall *HF* splittings could not be fitted to the calculated ones within the experimental uncertainty. A good fit could be obtained by the introduction of the terms $\sum A_i' S_i^3 I_i$. Although we do not understand very well the physical meaning of these terms, and especially how they can be so large, we have added them to the Hamiltonian in order to indicate what

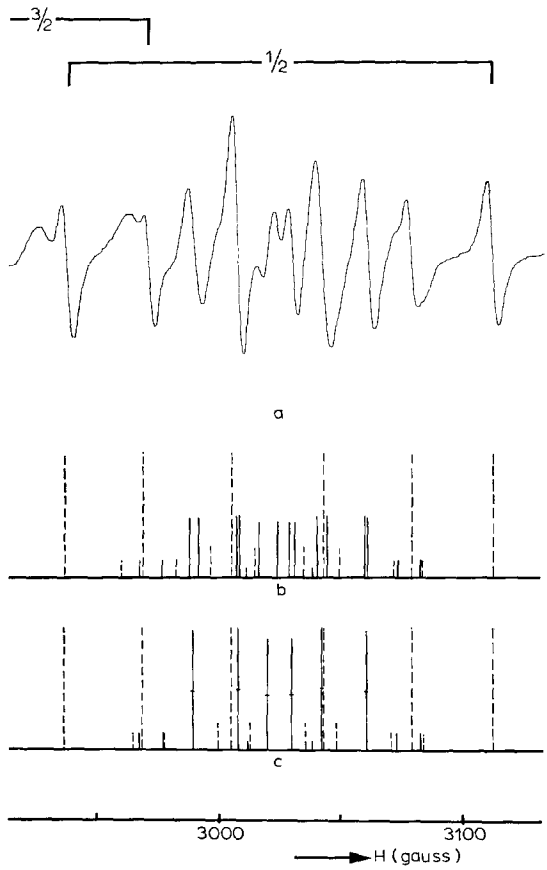

Fig. 7. Hyperfine structure of the electronic transition $M = \frac{1}{2} \leftrightarrow M = -\frac{1}{2}$ for the magnetic field parallel to the *a* axis.

(*a*) The experimental result. At the low magnetic field side there is some overlap with the *HF* lines of the transition $M = \frac{3}{2} \leftrightarrow M = \frac{1}{2}$.

(*b*) Position and intensity of the *HF* lines calculated from the nuclear part of the spin Hamiltonian (3). Dashed lines for ^{151}Eu and solid lines for ^{153}Eu.

(*c*) Position and intensity of the *HF* lines calculated from the nuclear part of the spin Hamiltonian if the terms in g_I and Q_1 are neglected.

the deviations are. Table III demonstrates the deviation that exist for $H||z$ axis if we require $A_z' = 0$ and the good fit obtained when we allow A_z' to take on the optimum value $^{151}A_z' = 0.11 \times 10^{-4}$ cm^{-1}. The determination of the parameters $^{153}Q_1$ and $|^{153}Q_2|$ by the method described in sec. 4 is illustrated in fig. 7. The experimentally observed *HFS* of the transition $M = \frac{1}{2} \leftrightarrow M = -\frac{1}{2}$ (fig. 7*a*) is compared with the spectrum calculated when in (3) the terms in Q_1 and g_I are neglected (fig. 7*c*) and with that calculated when these terms are included (fig. 7*b*). There is a detailed agreement between the latter and the observed spectrum.

6. *Shielding factors.* The parameters Q_1 and Q_2 are related to the crystalline electric field coefficients C_2^0, C_2^2 by the equation:

$$Q_{1,2} = \frac{eQ}{I(2I-1)}(1 - \gamma_\infty)C_2^{0,2} \tag{5}$$

where e is the proton charge, Q the nuclear quadrupole moment, I the nuclear spin and γ_∞ the antishielding factor. (Since Eu^{2+} is in a *S*-state, the direct interaction between the 4*f*-shell and the nuclear quadrupole is negligible; the 4*f* electrons do, of course, contribute to γ_∞.) In crystal field theory, fine structure splittings are determined by quantities

$$(1 - \gamma_l)A_l^m\langle r^l\rangle = -e(1 - \gamma_l)C_l^m\langle r^l\rangle$$

where the γ_l are again shielding factors and $\langle r^l\rangle$ is the mean value of r^l for the 4*f* electrons. Reasonably accurate values of $\langle r^2\rangle$ are available[27]), so that if we could derive the quantities $(1 - \gamma_2)A_2^{0,2}\langle r^2\rangle$ from the experimental data we would be able to determine the ratio $(1 - \gamma_\infty)/(1 - \gamma_2)$. Also, since we calculated C_2^0 and C_2^2 in the point charge approximation we could find $(1 - \gamma_\infty)$ and $(1 - \gamma_2)$ separately, but these values would be less reliable because the point charge approximation is known to be rather crude.

Unfortunately, the products $(1 - \gamma_l)A_l^m\langle r^l\rangle$ cannot be derived unambiguously from the experimental data for an *S*-state. The best we can do is to investigate how far the experimental values of b_2^0 and b_2^2 can be understood on the basis of existing theories and which value of $(1 - \gamma_2) \cdot A_2^{0,2}\langle r^2\rangle$ is compatible with such an interpretation. In developing our interpretation we shall keep our assumptions as simple and as limited in number as possible.

The relative sign of $^{153}Q_2$ could not be determined from the experiments. However, we find $^{153}Q_1$ to be positive, whereas C_2^0/C_2^2 was calculated as negative. We therefore expect $^{153}Q_2$ to be negative. We now remark that:

a. The principal axes of the second degree part of the crystal field terms in the spin Hamiltonian nearly coincide with the principal axes of the

crystal field gradient as calculated in the point charge approximation (see fig. 1).

b. b_2^0/b_2^2 has the same sign and the same order of magnitude as Q_1/Q_2.

These facts suggest that crystal field terms in A_2^0 and A_2^2 give the main contributions to to b_2^0 and b_2^2 and that the relation between them is mainly linear. If we now assume that b_2^0 and b_2^2 are functions only of A_2^0 and A_2^2 we may calculate to which extent linear effects contribute to b_2^0 and b_2^2 with the help of a relation established in appendix B. The result is that b_2^2 depends linearly on A_2^2 to an amount of approximately -500×10^{-4} cm^{-1}. A linear relation between b_2^0 and A_2^0 for axial crystals is predicted by perturbation mechanisms proposed by Pryce[3]) and Elliott and Stevens[4]). The latter mechanism works via the admixture of the $^6P_{7/2}$ excited state into the $^8S_{7/2}$ ground state by spin-orbit coupling. From the g value it is estimated that this admixture is quite sizeable for Eu^{2+} (see sec. 7) and we therefore investigate how far this perturbation may account for the fine structure splitting. For this perturbation the quantitative relation between b_2^0 and A_2^0 in axial crystals has been given by Hutchison *e.a.*[2]). According to our result in appendix B this same relation should hold between b_2^2 and A_2^2:

$$b_2^2 = -\frac{12}{5}\frac{\zeta^3}{W_P^2 W_D}(1-\gamma_2)A_2^2\langle r^2\rangle$$

where ζ is the one electron spin-orbit parameter, W_P and W_D are the energies of the levels $^6P_{7/2}$ and $^6D_{7/2}$ relative to the ground state level $^8S_{7/2}$. From the g value it is estimated (see sec. 7) $14\zeta^2/W_P^2 = 0.029$. Judd and Lindgren[28]) calculated $\zeta = 1361$ cm^{-1} for Eu^{3+} and $\zeta = 1228$ cm^{-1} for Eu. Interpolating linearly we estimate $\zeta = 1316$ cm^{-1} for Eu^{2+}. This then leads to $W_P = 29{,}400$ cm^{-1} which compares reasonably with the known value $W_P = 32{,}200$ cm^{-1} for Gd^{3+}[29]). We estimate $W_D \approx 32{,}000$ cm^{-1} for Eu^{2+}. Taking $b_2^2 = -500 \times 10^{-4}$ cm^{-1} (this is what we estimated to be the linear contribution to b_2^2) and $\langle r^2\rangle = 0.938 a_0^2$[27]) we find $(1-\gamma_2)A_2^2 = 261$ cm$^{-1}/a_0^2$. From this, and the value of the quadrupole interaction parameter Q_2 we finally derive $(1-\gamma_\infty)/(1-\gamma_2) = 169$.

The above line of argument for the derivation of the ratio $(1-\gamma_\infty)/(1-\gamma_2)$ for Eu^{2+} from the *PMR* results can be summarized as follows. The value of the largest crystal field parameter, b_2^2, in the spin Hamiltonian for Eu^{2+} in $PbCl_2$ can be reasonably understood on the basis of a perturbation mechanism proposed by Elliott and Stevens, cubic in spin-orbit interaction and linear in the second degree crystal field coefficients assuming the ratio $(1-\gamma_\infty)/(1-\gamma_2)$ to be equal to 169.

Using the calculated value of C_2^2 we find furthermore $\gamma_\infty = -114$ and $\gamma_2 = 0.32$. As stated above, not too much credit can be given to these figures.

7. *Discussion.* Signs of parameters. Only relative signs of the parameters could be determined. However, there is some evidence that the signs given are the correct ones. First, we find the nuclear parameter A to be negative. Baker e.a.[22]) found A to be negative for Eu^{2+} in CaF_2. Since A does not vary greatly from crystal to crystal one would expect it to be negative in our case too. Secondly, we find a negative value for the antishielding factor, in agreement with theoretical predictions.

g values. Within the accuracy of the measurements, the g value is isotropic and equal to the more precise value $g = 1.9926 \pm 0.0003$ found by Baker and Williams for Eu^{2+} in CaF_2. These authors attributed the deviation of this g value from that for the pure $^8S_{7/2}$ state corrected for relativistic and diamagnetic effects to an admixture of the $^6P_{7/2}$ state by spin-orbit coupling. From the experimental value they deduced $14\zeta^2/W_P^2 = 0.029 \pm 0.001$, where ζ is the spin-orbit coupling parameter and W_P the energy of the $^6P_{7/2}$ state relative to the $^8S_{7/2}$ ground state. The admixture of $^6P_{7/2}$ plays an important part in the second degree crystal field splittings. The ratio ζ^2/W_P^2 as given above was used in the interpretation of these splittings in sec. 6.

Hyperfine structure. It is clear from table III that the experimental data for the overall hyperfine splittings of ^{151}Eu cannot be fitted satisfactorily to the spin Hamiltonian when the terms $\sum_i A_i' S_i^3 I_i$ are omitted. After introduction of these terms a good fit can be obtained. It is noteworthy that the crystal field splittings are more or less axial around the x axis. If we take x, y, and z axis successively as axes of quantization, the corresponding b_2^0 values are $-318 \times 10^{-4}\,cm^{-1}$, $+209 \times 10^{-4}\,cm^{-1}$ and $+107 \times 10^{-4}\,cm^{-1}$. For A_x', A_y', A_z' we found $-0.10 \times 10^{-4}\,cm^{-1}$, $+0.10 \times 10^{-4}\,cm^{-1}$ and $+0.11 \times 10^{-4}\,cm^{-1}$. This suggests that the contribution $\sum_i A_i' S_i^3 I_i$ might have to do with an influence of the crystalline electric field on the hyperfine interaction. This influence would then be unexpectedly large[30]). To the authors' knowledge no other *PMR* investigations of Eu^{2+} in noncubic fields have as yet been published. Such studies might be interesting in view of the anomaly discussed above.

Shielding factors. Crystal field splittings of the electronic levels of the rare earth ions are known to be small compared to those for iron group ions. For a long time already this has been considered to be the result of a shielding of the external potential, mainly by the outermost $5s^2p^6$ electrons. Judd[31]) supposed such a shielding to be responsible for the relatively small values of $(1 - \gamma_2)\, A_2^0 \langle r^2 \rangle$ found experimentally in lanthanum ethylsulphate and trichloride.

Recently the shielding effects in rare earth ions have become the subject of several quantitative studies, both theoretical and experimental. Wikner and Burns[32]) made a theoretical estimate of γ_∞ for the trivalent rare earth ions. They arrived at a value of γ_∞ that varies with atomic number

from -80 for Ce^{3+} to about -50 for Yb^{3+}. Burns[6]) calculated $(1-\gamma_2)$ for K^+ and found $(1-\gamma_2) \approx 0.88$. From this he concluded that shielding effects play only a minor part and that the small crystal field splittings are rather a result of large spin-orbit coupling and large physical size of the rare earth ions and the weakness of the crystal fields in the crystals in which these ions are embedded. Later theoretical work, however, consistently indicates the presence of a substantial shielding, γ_2 being of the order of magnitude of 0.50 or larger.

Ray[33]) made calculations of both γ_∞ and γ_2 for Pr^{3+}. His result for γ_2 $(= 0.52)$ is close to that of other recent calculations, but his value for γ_∞ $(= -16.37)$ is appreciably smaller than those obtained by Wikner and Burns and Watson and Freeman[34]). Lenander and Wong[35]) calculated the shielding factor γ_2, again for Pr^{3+}. They find $\gamma_2 = 0.59$ and argue that it might be considerably larger. Recently Watson and Freeman[30]) also considered the shielding problem. These authors show that there can be a considerable nonlinear shielding, which means that the effective potential for the $4f$-electrons does not have the same symmetry as the external potential (e.g. for an external V_4^0 potential the polarization of closed shells may give V_2^0 and V_6^0 contributions to the energy level scheme). This effect is not large, however, for a V_2^0 potential for which there is essentially linear shielding and $\gamma_2 \approx 0.50$. Watson and Freeman[34]) also calculated γ_∞ and for the ions La^{3+}, Ce^{3+}, Yb^{3+} they found the values -68, -71, and -79 respectively.

Summarizing these results it seems fair to say that at present the theory predicts for the trivalent rare earth ions an antishielding factor γ_∞ of about -80 and a shielding factor $\gamma_2 \approx 0.50$ or possibly larger.

As we have seen in sec. 6 the ratio $(1-\gamma_\infty)/(1-\gamma_2)$ can be derived from the experiments more reliably than either $(1-\gamma_\infty)$ or $(1-\gamma_2)$, because of the uncertainties involved in determining the crystalline electric fields. Edmonds[36]) measured the quadrupole interaction of the La nucleus in lanthanum trichloride, magnesium nitrate and ethylsulphate. From the experimental values of $(1-\gamma_2)A_2^0\langle r^2\rangle$ for various rare earth ions in these salts Freeman and Watson[27]) calculated the corresponding $(1-\gamma_2)A_2^0$ using their values of $\langle r^2\rangle$. Extrapolating these $(1-\gamma_2)A_2^0$ values to the La^{3+} ion Edmonds finds $(1-\gamma_\infty)/(1-\gamma_2) = 550$ in the ethysulphate and $= 350$ in the trichloride. Barnes *e.a.*[37])[38]) studied the temperature dependence of the quadrupole splitting in thulium ethylsulphate and thulium oxide. Their analysis yields $(1-\gamma_\infty)/(1-\gamma_2) = = 250$ and $= 130$ in these cases respectively.

From our measurements we inferred $(1-\gamma_\infty)/(1-\gamma_2) = 169$ which is in remarkable agreement with theoretical estimates. Using the computed values of the crystal field gradient we furthermore found $\gamma_\infty = -114 \pm 18$. Since the theoretical calculations suggest that γ_∞ should be approximately

-80, this indicates that the calculation of the crystalline electric field in the point charge approximation gives a fairly good result in the present case.

Conclusion. The measurement of the *PMR* spectra of Eu^{2+} in an environment of monoclinic symmetry enabled us to compare the fine structure splittings with the nuclear quadrupole splittings and the calculated value of the crystal field gradient. The fine structure splittings are mainly of the second degree and they can be quite well accounted for by a perturbation mechanism proposed by Elliott and Stevens[4]), assuming a ratio $(1-\gamma_\infty)/(1-\gamma_2) = 169$, where γ_∞ is the antishielding factor and γ_2 the second degree shielding factor for the $4f$ electrons. This value of $(1-\gamma_\infty)/(1-\gamma_2)$ is in good agreement with recent theoretical estimates. Using the theoretical estimate $\gamma_\infty \approx -80$ and the experimental values of the nuclear quadrupole splitting it is found that the calculation of the crystal field gradient in the point charge approximation gives a surprisingly good result in the present case.

Acknowledgements. The authors would like to thank Prof. Dr. B. R. A. Nijboer, Dr. F. W. de Wette, Dr. J. S. van Wieringen and Dr. A. J. Freeman for helpful discussions, Mr. K. J. de Vries for preparing single crystals of $PbCl_2$ containing small amounts of Eu, Dr. H. J. Endeman for X ray measurements on these crystals, Mr. C. A. Ch. Görts for help with the computations on the university's computer and Mr. J. M. Trooster and Mr. G. H. Bardelmeyer for performing part of the measurements.

APPENDIX A

The operators O_l^m and O_l^{-m} used in the spin Hamiltonian (3) are the operator equivalents[16]) of the functions $r^l\Phi_l^m$ and $r^l\Phi_l^{-m}$ where

$$\Phi_l^m(\theta, \varphi) = 2\alpha_l^m \operatorname{Re}(Y_l^m(\theta, \varphi))$$

$$\Phi_l^{-m}(\theta, \varphi) = 2\alpha_l^m \operatorname{Im}(Y_l^m(\theta, \varphi))$$

The α_l^m are constants given in table IV for $l = 2, 4, 6$ and $m = 0, 1, \ldots l$.

In cases where the crystal field energy is small compared to the Zeeman energy the energy levels can be calculated by a perturbation expansion, the zeroth order functions being the eigenfunctions of S_z where z is chosen along the direction of magnetization. The crystal field part of the spin Hamiltonian should now be written on this new z axis, which requires a transformation of the O_l^m and O_l^{-m}. Such transformations have been considered by various authors[39–41]). Let the new coordinate system $OXYZ$

TABLE IV

The numerical factors α_l^m			
m	$\sqrt{\frac{5}{4\pi}}\,\alpha_2^m$	$\sqrt{\frac{9}{4\pi}}\,\alpha_4^m$	$\sqrt{\frac{13}{4\pi}}\,\alpha_6^m$
0	1	4	8
1	$-\frac{1}{\sqrt{6}}$	$-\frac{2}{\sqrt{5}}$	$-\frac{8}{\sqrt{42}}$
2	$\frac{2}{\sqrt{6}}$	$\frac{4}{\sqrt{10}}$	$\frac{16}{\sqrt{105}}$
3		$-\frac{2}{\sqrt{35}}$	$-\frac{8}{\sqrt{105}}$
4		$\frac{8}{\sqrt{70}}$	$\frac{16}{\sqrt{14}}$
5			$-\frac{8}{\sqrt{693}}$
6			$\frac{16}{\sqrt{231}}$

have polar angles (θ, φ) relative to the old one $Oxyz$. We then have:

$$(O_l^m)' = D_{0m}^{l+}(\theta)O_l^0 \cos m\varphi + \sum_{m'=1}^{l} \{D_{m'm}^{l+}(\theta)O_l^{m'} \cos m\varphi + D_{m'm}^{l-}(\theta)O_l^{-m'} \sin m\varphi\} \tag{6}$$

$$(O_l^{-m})' = D_{0m}^{l+}(\theta)O_l^0 \sin m\varphi + \sum_{m=1}^{l} \{D_{m'm}^{l+}(\theta)O_l^{m'} \sin m\varphi - D_{m'm}^{l-}(\theta)O_l^{-m'} \cos m\varphi\} \tag{7}$$

The coefficients $D_{m'm}^{l\pm}$ have been calculated numerically by Baker[40] and are reproduced graphically in his paper. Simple goniometric expressions were derived by Vrehen[1] for $l = 2, 4, 6$ and m even.

Be $E_c^1(M)$ and $E_c^2(M)$ first and second order crystal field energies for the state $|M\rangle$ and $E^0(M)$ the unperturbed (= Zeeman) energy. One then has

$$E_c^1(M) = \sum_{l,m} D_{0m}^{l+}(\theta)\{B_l^m \cos m\varphi + B_l^{-m} \sin m\varphi\}\langle M|O_l|M\rangle \tag{8}$$

$$E_c^2(M) = \sum_{m_0 \neq 0} \frac{|\langle M + m_0|\mathscr{H}_c|M\rangle|^2}{E^0(M) - E^0(M + m_0)} \tag{9}$$

where

$$|\langle M + m_0|\mathscr{H}_c|M\rangle|^2 = \sum_{ll'} \{\langle M + m_0|O_l^{|m_0|}|M\rangle\langle M|O_{l'}^{|m_0|}|M + m_0\rangle\} \cdot \sum_{m'm} (B_l^m B_{l'}^{m'} p + 2B_l^m B_{l'}^{-m'} q + B_l^{-m} B_{l'}^{-m'} r).$$

$$\begin{aligned} p &= A \cos (m + m')\varphi + B \cos (m - m')\varphi \\ q &= A \sin (m + m')\varphi - B \sin (m - m')\varphi \\ r &= -A \cos (m + m')\varphi + B \cos (m - m')\varphi \end{aligned}$$

$$A = A(m_0, m, l, m', l') = \tfrac{1}{2}(D^{l+}_{|m_0|m} D^{l'+}_{|m_0|m'} - D^{l-}_{|m_0|m} D^{l'-}_{|m_0|m'})$$
$$B = B(m_0, m, l, m', l') = \tfrac{1}{2}(D^{l+}_{|m_0|m} D^{l'+}_{|m_0|m'} + D^{l-}_{|m_0|m} D^{l'-}_{|m_0|m'})$$

The expressions (8) (9) were used in the analysis of the angular variation of the resonance lines for Eu^{2+} in $PbCl_2$ in the *bc* plane (see sec. 4).

APPENDIX B

Generally, the parameters B_2^0 and B_2^2 in the spin Hamiltonian need not necessarily be functions of the crystal field coefficients A_2^0 and A_2^2 only. For instance, for an iron group ion with $L \neq 0$ in a cubic crystal field with a small axial distortion B_2^0 will depend on the cubic component as well. Also, Judd[5]) has shown that for Gd^{3+} in axial crystals higher order crystal field coefficients may contribute to B_2^0. However, for the configuration $^6S_{5/2}$ in axial fields, data have been analyzed under the assumption that B_2^0 depends on A_2^0 (rather on $(1 - \gamma_2)A_2^0\langle r^2\rangle$, but for simplicity we write A_2^0) only and perturbation mechanisms have been studied that are linear and quadratic in A_2^0[42])[43]). In this appendix we show how the relations between B_2^0 and A_2^0 in axial crystals can be generalized to relations between B_2^0, B_2^2, and A_2^0, A_2^2 for lower symmetries if the $B_2^{\pm m}$ depend only on the $A_2^{\pm m}$.

We can always choose a coordinate system in such a way that from the $A_2^{\pm m}$ only A_2^0 and A_2^2 do not vanish. Since we assume the $B_2^{\pm m}$ to be functions of the $A_2^{\pm m}$ only, all the $B_2^{\pm m}$ then vanish for symmetry reasons except B_2^0 and B_2^2. The most general quadratic relation between B_2^0, B_2^2 and A_2^0, A_2^2 can be written:

$$B_2^0 = \alpha' A_2^{0^2} + \beta' A_2^0 A_2^2 + \gamma' A_2^{2^2} + \delta' A_2^0 + \varepsilon' A_2^2 \tag{10}$$
$$B_2^2 = \alpha'' A_2^{0^2} + \beta'' A_2^0 A_2^2 + \gamma'' A_2^{2^2} + \delta'' A_2^0 + \varepsilon'' A_2^2 \tag{11}$$

Now the coordinate system may be chosen in several ways so that only A_2^0 and A_2^2 are different from zero, i.e., x, y, and z axis may be interchanged and this leads to different sets A_2^0, A_2^2 and B_2^0, B_2^2. If we require that the relations (10) (11) hold between (B_2^0, B_2^2) and (A_2^0, A_2^2) for each of these sets we find that (10) and (11) reduce to

$$B_2^0 = \alpha'(A_2^{0^2} - \tfrac{1}{3}A_2^{2^2}) + \delta' A_2^0 \tag{12}$$
$$B_2^2 = -2\alpha' A_2^0 A_2^2 + \delta' A_2^2 \tag{13}$$

When only a linear mechanism contributes $B_2^0/B_2^2 = A_2^0/A_2^2$. If quadratic terms are also present we may calculate the linear and quadratic contributions with the relations (12) and (13). These relations were used in sec. 6 to estimate the linear contribution to B_2^2.

Received 17-10-64

REFERENCES

1) Vrehen, Q. H. F., thesis, Utrecht (1963).
2) Hutchison, C. A., Judd, B. R. and Pope, D. F. D., Proc. Phys. Soc. **B70** (1957) 514.
3) Pryce, M. H. L., Phys. Rev. **80** (1950) 1107.
4) Elliott, R. J. and Stevens, K. W. H., Proc. Roy. Soc. **A219** (1953) 387.
5) See ref. 2.
6) Burns, G., Phys. Rev. **128** (1962) 2121.
7) Garwin, R. L., Rev. sci. Instr. **29** (1958) 223.
8) Garwin, R. L., Hutchinson, D., Penman, S. and Shapiro, G., Rev. sci. Instr. **30** (1959) 105.
9) Groth, P., Chemische Cristallographie I, Engelman, Leipzig (1906) 219.
10) Braekken, H., Z. Krist. **83** (1932) 222.
11) Sahl, K. und Zemann, J., Naturwissenschaften **48** (1961) 641.
12) De Wette, F. W. and Nijboer, B. R. A., Physica **24** (1958) 1105.
13) Hiller, J. E., Grundriss der Kristallchemie, W. de Gruyter, Berlin (1952) 145.
14) Wyckoff, R. W. G., Crystal Structures, Interscience, New York (1948).
15) Ketelaar, J. A. A., De Chemische Binding, Elsevier, Amsterdam (1952).
16) Stevens, K. W. H., Proc. Phys. Soc. **A65** (1952) 209.
17) Elliott, R. J. and Stevens, K. W. H., Proc. Roy. Soc. **A218** (1953) 553.
18) Judd, B. R., Proc. Roy. Soc. **A227** (1955) 552.
19) Baker, J. M., Bleaney, B. and Hayes, W., Proc. Roy. Soc. **A247** (1958) 141.
20) Jones, D. A., Baker, J. M. and Pope, D. F. D., Proc. Phys. Soc. **74** (1959) 249.
21) Orbach, R., Proc. Roy. Soc. **A264** (1961) 458.
22) Baker, J. M. and Williams, F. I. B., Proc. Roy. Soc. **A267** (1962) 283.
23) Krebs, K. und Winkler, R., Naturwissenschaften **47** (1960) 490.
24) Bleaney, B., Phil. Mag. **42** (1951) 441.
25) Lacroix, R., Helv. Phys. Acta **30** (1957) 374.
26) Bleaney, B. and Rubins, R. S., Proc. Phys. Soc. **77** (1961) 103; ibidem **78** (1961) 778.
27) Freeman, A. J. and Watson, R. E., Phys. Rev. **127** (1962) 2058.
28) Judd, B. R. and Lindgren, I., Phys. Rev. **122** (1961) 1802.
29) McClure, D. S., Solid State Physics **9** (1959) 399.
30) Watson, R. E. and Freeman, A. J., Phys. Rev. **133** (1964) A1571.
31) Judd, B. R., Proc. Roy. Soc. **A251** (1959) 134.
32) Wikner, E. G. and Burns, G., Phys. Letters **2** (1962) 225.
33) Ray, D. K., Proc. Phys. Soc. **82** (1963) 47.
34) Watson, R. E. and Freeman, A. J., Phys. Rev. **135** (1964) A1209.
35) Lenander, C. J. and Wong, E. Y., J. chem. Phys. **38** (1963) 2750.
36) Edmonds, D. T., Phys. Rev. Letters **10** (1963) 129.
37) Barnes, R. G., Kankeleit, E., Mössbauer, R. L. and Poindexter, J. M., Phys. Rev. Letters **11** (1963) 253.
38) Barnes, R. G., Mössbauer, R. L., Kankeleit, E. and Poindexter, J. M., Phys. Rev. **136** (1964) A175.
39) Sachs, M., J. Phys. Chem. Solids **15** (1960) 291.
40) Baker, J. M. and Williams, F. I. B., Proc. Phys. Soc. **78** (1961) 1340.
41) Buckmaster, H. A., Canad. J. Phys. **40** (1962) 1670.
42) Watanabe, H., Progr. theor. Phys. **18** (1957) 405.
43) Germanier, A. M., Gainon, D. and Lacroix, R., Phys. Letters **2** (1962) 105.